Singer, B., & Grunberger, D. (1983) *Molecular Biology of Mutagens and Carcinogens*, Plenum Press, New York.
Tang, M.-S., & Lieberman, M. W. (1983) *Carcinogenesis 4*, 1001-1006.
Voigt, J. M., Van Houten, B., Sancar, A., & Topal, M. D. (1989) *J. Biol. Chem. 264*, 5172-5176.
Warpehoski, M. A., & Hurley, L. H. (1988) *Chem. Res. Toxicol. 1*, 315-333.
Weeks, C. E., Allaben, W. T., Tresp, N. M., Louie, S. C., Lazear, E. J., & King, C. M. (1980) *Cancer Res. 40*, 1204-1211.
Westra, J. G. (1981) *Carcinogenesis 2*, 355-357.

Physical Studies of DNA Premelting Equilibria in Duplexes with and without Homo dA·dT Tracts: Correlations with DNA Bending†

Shirley S. Chan* and Kenneth J. Breslauer*
Department of Chemistry, Rutgers, The State University of New Jersey, New Brunswick, New Jersey 08903
Michael E. Hogan and Donald J. Kessler
Center for Biotechnology, Baylor College of Medicine, The Woodlands, Texas 77381
Robert H. Austin, Jeff Ojemann, Jonathan M. Passner, and Nada C. Wiles
Department of Physics, Princeton University, Princeton, New Jersey 08544
Received December 26, 1989; Revised Manuscript Received April 2, 1990

ABSTRACT: We have employed a variety of physical methods to study the equilibrium melting and temperature-dependent conformational dynamics of dA·dT tracts in fractionated synthetic DNA polymers and in well-defined fragments of kinetoplast DNA (kDNA). Using circular dichroism (CD), we have detected a temperature-dependent, "premelting" event in poly(dA)·poly(dT) which exhibits a midpoint near 37 °C. Significantly, we also detect this CD "premelting" behavior in a fragment of kDNA. By contrast, we do not observe this "premelting" behavior in the temperature-dependent CD spectra of poly[d(AT)]·poly[d(AT)], poly(dG)·poly(dC), poly[d(GC)]·poly[d(GC)], or calf thymus DNA. Thus, poly(dA)·poly(dT) and kDNA exhibit a common CD-detected "premelting" event which is absent in the other duplex systems studied in this work. Furthermore, we find that the anomalous electrophoretic retardation of the kDNA fragments we have investigated disappears at temperatures above approximately 37 °C. We also observe that the rotational dynamics of poly(dA)·poly(dT) and kDNA as assessed by singlet depletion anisotropy decay (SDAD) and electric birefringence decay (EBD) also display a discontinuity near 37 °C, which is not observed for the other duplex systems studied. Thus, in the aggregate, our static and dynamic measurements suggest that the homo dA·dT sequence element [common to both poly(dA)·poly(dT) and kDNA] is capable of a temperature-dependent equilibrium between at least two helical states in a temperature range well below that required to induce global melting of the host duplex. We suggest that this "preglobal" melting event may correspond to the thermally induced "disruption" of "bent" DNA.

Crystal structures of proteins, nucleic acids, and their complexes have provided valuable structural frameworks for developing an understanding of the interactions that control gene regulation. However, by its very nature, crystallography emphasizes the static or, at best, the time-averaged structure of a macromolecule. As a result, models for site-specific binding events often have a "lock and key" quality that tries to explain recognition in terms of rigid partners. One example of such thinking is the proposal that certain sequences of DNA are "bent" (Nelson et al., 1987; Coll et al., 1987; Alexeev et al., 1987). To be specific, the slow electrodiffusion constant in polyacrylamide gels of helices with periodic arrays of homo dA·dT segments [e.g., kinetoplast DNA (kDNA)] has been interpreted as the effect of a static curvature of the helix (Diekmann & Wang, 1985; Woo & Crothers, 1984). In addition, certain aspects of gene regulation may involve the binding-induced physical distortion of the DNA helix away from a linear "B" form (Frederick et al., 1984; Liu-Johnson et al., 1986; Hogan et al., 1987). Consequently, certain sequences of DNA may be statically bent while other sequences inherently may be more deformable (elastic). Identifying and distinguishing between these two classes of DNA "bending" should be of importance in our understanding of ligand-DNA interactions as well as in our understanding of the influence of sequence on DNA structure.

In this paper we examine several physical aspects of the unusual properties of the homopolymer poly(dA)·poly(dT), since it is believed that this particular sequence motif is closely related to many aspects of "bent" DNA and the abnormalities exhibited by kDNA (Srinivasan et al., 1987; Maroun & Olson, 1988). We note the similarities in several "premelting" physical properties of poly(dA)·poly(dT) and kDNA and contrast these properties with those of other synthetic and natural DNA duplexes which do not contain homo dA·dT tracts (also called "A tracts"). The "premelting" properties we report are to be differentiated from those associated with the large body of previous studies on DNA premelting [Doty et al., 1959; Ts'o & Helmkamp, 1961; Fresco, 1961; Freund

† We gratefully acknowledge the support of the Office of Naval Research (N00014-86-K-0263) to R.H.A., the National Science Foundation (DMB8816340) to R.H.A., the National Cancer Institute (USPH2R01CA39527-04/08) to M.E.H., and the National Institutes of Health (GM23509 and GM34469) to K.J.B.
* To whom correspondence should be addressed.

0006-2960/90/0429-6161$02.50/0

& Bernardi, 1963; Lazurkin et al., 1970; von Hippel & Wong, 1971; Gennis & Cantor, 1972; Crothers et al., 1973; Erfurth & Peticolas, 1975; Brahms et al., 1976; Greve et al., 1977; Palecek (1976) and references cited therein]. These earlier studies generally employed unfractionated samples, focused primarily on optical properties at lower temperatures, did not include parallel electrophoretic and/or dynamic studies, and did not have the opportunity to compare the observed premelting properties with those of kDNA, particularly in the context of the relatively recent concept of DNA bending (Olson et al., 1987). Our aim in this work is to begin to develop a base of experimental data from measurements under physiological conditions that can be used to develop insight into equilibrium and dynamic aspects of DNA bending. To conduct the required measurements, we have employed two different approaches: static measurements, which are sensitive to structural/conformational changes in the DNA fragments, and dynamic measurements, which are sensitive to both structural/conformational changes and changes in the elastic properties of the helix. Such a two-pronged attack is necessary since it appears that the interaction of DNA with proteins involves both static aspects *and* elastic deformations (Srinivasan et al., 1987; Maroun & Olson, 1988). Our experimental data reveal the following significant trends:

(1) The temperature dependence of the circular dichroism (CD) spectrum of both fractionated and unfractionated poly(dA)·poly(dT) sequences exhibits a thermally induced "premelting" event which occurs prior to the global duplex to single strand transition. The van't Hoff enthalpy change associated with this broad premelting transition is ~20 kcal/mol of cooperative unit.

(2) The temperature dependence of the CD measurements on well-defined kinetoplast DNA (kDNA) fragments [containing about 40% homo oligo(dA)·oligo(dT) segments] also shows a gradual premelting process prior to global melting similar to that observed for poly(dA)·poly(dT). By contrast, calf thymus DNA, and other synthetic DNAs which do not contain periodic A tracts, do not exhibit a CD-detected, premelting process prior to global melting.

(3) The anomalous electrophoretic properties of kDNA fragments disappear with increasing temperature. In fact, we find that the thermal disruption of the anamolous electrophoretic mobility of kDNA occurs over the same temperature range as the CD-detected, thermally induced transitions we observe in poly(dA)·poly(dT) and kDNA fragments.

(4) Singlet depletion anisotropy decay (SDAD) and electric birefringence (EBR) measurements reveal that the unusual static properties of poly(dA)·poly(dT) also impart rigidity changes or conformational changes that result in unusual rotational diffusions. (These techniques are particularly sensitive to the large-scale, collective motions of the macromolecule.) Both techniques detect a temperature-dependent transition in the dynamical properties of poly(dA)·poly(dT) and kDNA. In fact, for poly(dA)·poly(dT), the temperature dependence of the anisotropy decay reveals a broad transition of equivalent breadth and midpoint as that which we observe in our temperature-dependent CD and electrophoretic mobility measurements.

A detailed modeling of the dynamic results will be presented independently (R. H. Austin and M. E. Hogan, unpublished results). In this paper we emphasize the temperature-dependent equilibrium properties of a series of DNA duplexes both with and without A tracts. In particular, we emphasize the presence of a "premelting" transition in poly(dA)·poly(dT) and kDNA which is absent in other DNA duplexes without A tracts and which occurs at a temperature close to that which is required to impart normal electrophoretic behavior to kDNA.

Materials and Methods

DNA Purification. Long DNA polymers were fractionated and separated, and then the lengths of the isolated samples were measured. These samples enabled us to study DNA molecules with similar lengths, but different sequences. For natural DNAs, we have used restriction enzymes to provide specific sequences of known length.

Polynucleotides were purchased from Boehringer Mannheim, suspended in 1 × TE buffer (10 mM Tris-HCl, 1 mM EDTA, pH 7.6), incubated at 20 °C below the T_m to optimize duplex hybridization, and then sonicated at 4 °C, for 15 min. The resulting material was deproteinized with phenol, ethanol precipitated, resuspended in TE buffer, and then fractionated by high-precision Sephacryl S-500 matrix exclusion chromatography using a 100-cm column, eluting with 50 mM Tris-HCl and 1 mM EDTA, pH 7.6.

The DNA average lengths were determined by measuring gel mobility relative to the *Eco*RI + *Ava*II digest of pBR322, by electrophoresis on native 4% and 8% polyacrylamide gels [29/1 acrylamide/bis(acrylamide) ratio], by denaturing electrophoresis in a 2% agarose gel, and/or by analytical ion-exchange HPLC on a GEN-PAK FAX column (Waters). Relative to random sequence length standards, we found that the apparent length of such fractions is independent of the gel assay system and that the individual fractions narrowly distribute about an average length with a width of about 10%. Thus, we are confident that we have properly accounted for DNA length. From quantitative analysis of the electrophoresis data, we estimate the following median lengths for the fractions used in the spectroscopic studies: poly(dA)·poly(dT), 520 bp, 780 bp, and >1000 bp (nonfractionated); poly[d(AT)]·poly[d(AT)], 810 bp; poly(dG)·poly(dC), 400 bp; poly[d(GC)]·poly[d(GC)], 460 bp; kDNA, 265 bp; calf thymus DNA, 300 bp. The median lengths of the samples used in the SDAD and EBR studies for AT or GC homopolymers and alternating copolymers were 450 bp, 145 bp, or 210 bp with approximately one standard deviation from the mean for the AT polymers and with two standard deviations for the GC polymers.

Concentrations were determined spectroscopically by using the following 25 °C values in base-pair equivalents for ϵ_{260} (M^{-1} cm^{-1}): poly(dA)·poly(dT) = $12.0 \times 10^{+3}$; poly[d(AT)]·poly[d(AT)] = $13.3 \times 10^{+3}$; poly(dG)·poly(dC) = $12.7 \times 10^{+3}$; poly[d(GC)]·poly[d(GC)] = $16.8 \times 10^{+3}$; kDNA = $12.0 \times 10^{+3}$; calf thymus = $13.3 \times 10^{+3}$.

The DNA fragment of *Crithidia fasciculata* kinetoplast DNA was isolated from the plasmid pPK201/CAT, which was cloned by Paul Englund and colleagues (Kitchin et al., 1986). The 219 bp *Bam*HI–*Bam*HI kDNA insert was purified by preparative column electrophoresis on a 5% acrylamide matrix. We found this method has size resolution and capacity which is superior to exclusion chromatography. Material produced in this way is free of contaminants as assayed spectroscopically or biochemically because the columns can be electrophoresed exhaustively before loading DNA and because DNA electrophoreses through and then out of the matrix. The 209 bp 5S DNA fragment was isolated from the sea urchin plasmid p5S207, which was generated by Simpson and colleagues (Simpson & Stafford, 1983). Its 209 bp *Ava*I–*Ava*I insert (which is present as 18 copies in tandem) was purified by preparative electrophoresis, as above. Typical yields were 50 μg of pure 219 bp insert and 150 μg of pure 209 bp repeat per 4 L of bacterial culture. This amount of material is sufficient

for multiple SDAD and EBD measurements.

Gel Electrophoresis. The plasmid pPK201/CAT was linearized with *Eco*RI and then 3′ end labeled at the *Eco*RI termini with the Klenow fragment of DNA polymerase I, [^{32}P]dATP, and excess cold dTTP. Secondary cleavage was performed with *Hin*dIII, and the end-labeled kDNA fragment was isolated by column chromatography on a Sepharose 6B resin and equilibrated in 10 mM Tris-HCl, pH 8.0, with 0.05 mM EDTA.

The end-labeled kDNA fragment was then electrophoresed along with 3′ end labeled pBR322/*Hpa*II length markers in a native 7% polyacrylamide gel and in 45 mM Tris–borate buffer, pH 8.0, with 1 mM EDTA. In separate experiments, electrophoresis was performed at 4, 25, 30, 39, 47, 55, and 65 °C, as measured by the temperatures of the buffers in which the gels ran. Electrophoresis was allowed to proceed only after the gels and samples had equilibrated to the desired temperature. The relative mobility of the kDNA fragment was then measured at each temperature. The relative mobility is defined as the electrophoretic mobility of the kDNA fragment divided by the electrophoretic mobility of a marker fragment of the same length.

Circular Dichroism Measurements. The CD spectra were recorded on an Aviv spectropolarimeter (Aviv Associates, Model 60DS, Lakewood, NJ). Each spectrum shown is an average of three scans from 320 to 210 nm, with initial zeroing at 350 nm. All spectra were subtracted against a background scan with buffer. The spectral resolution was 0.5 nm/point and the bandwidth of each point was 1.5 nm. A rectangular quartz semimicrocuvette of 1-cm optical path length (especially selected for minimum birefringence) was used as the sample cell with a volume requirement of 1 mL. For precious samples like kDNA, we designed a Teflon cuvette with quartz windows with an optical path of 1 cm and a volume requirement of only 0.15 mL. The optical density (OD) at 260 nm of each sample ranged from 0.5 to 1.0. The synthetic polymers [except for the long poly(dA)·poly(dT) (>1000 bp) sample] were studied in a buffer consisting of 90 mM Tris-HCl, pH 7.6, with 10 μM Na-EDTA. EDTA concentration was kept low to avoid its absorbance at wavelengths below 220 nm. The long dA·dT sample (>1000 bp) was studied in 5 mM phosphate buffer, pH 7.0, thereby minimizing the formation of the triple helix. The kDNA and calf thymus DNA fragments were studied in 10 mM Tris-HCl buffer with 10 μM Na-EDTA, pH 7.6. The cuvette holder was temperature controlled by a Peltier effect heater/cooler. Each temperature measurement was equilibrated for at least 10 min. The adequacy of the equilibration time was verified by the absorption change at 260 nm. Reproducibility of the data was ensured by repetitive runs of the same sample.

Optical Absorption Measurement. Optical absorption measurements employed two different instruments to record the absorption spectra of the DNA samples as a function of temperature. In one method, temperature-dependent spectra were measured by using a conventional dual-beam spectrophotometer (Perkin-Elmer, Model Lamda 4C, Norwalk, CT) equipped with a Peltier heating device. In a second method, the absorption and the CD spectra of the samples were measured simultaneously at each temperature by using the single-beam Aviv 60DS spectropolarimeter. Corrected absorbance spectra were obtained by taking the log of the ratio of the sample spectrum to a blank buffer spectrum.

Melting curves were measured at 260 nm on a Perkin-Elmer spectrophotometer, Model 575, equipped with a translating, Peltier temperature-controlled cell holder which accommodates five cuvettes. The temperature and absorbance outputs of this spectrophotometer were interfaced to a Tektronix 4051 computer for data acquisition and processing. To ensure thermal equilibrium, the heating rate was set at 0.1 °C/min. All samples for UV melting were prepared at the same buffer conditions and similar concentrations as used to measure the CD spectra.

Three different conditions were used with the long dA·dT samples: (1) low concentration (OD = 0.8 at 260 nm) at low salt (5 mM); (2) low concentration (OD = 0.8 at 260 nm) at medium salt (100 mM); and (3) high concentration (OD = 16 at 260 nm) at medium salt (100 mM). For the high-concentration sample a quartz cuvette with an optical path of 0.1 cm was used. For each of the three conditions noted above, we recorded melting profiles for the long dA·dT sample at 260 and 280 nm between 10 and 80 °C.

Birefringence Measurements. Temperature-dependent measurements of free-field birefringence decays were conducted on the same DNA samples as were used in the CD experiments. A HeNe laser (632.8 nm) was used as the monitoring light source. The birefringence cell consists of a Teflon cell with a 100-μL volume. The electrodes are made of 2 mm by 8-mm gold strips with a 2-mm spacing between the plates. A Cober 100 pulse generator is employed to generate the field pulses. The pulse width was chosen to be typically 20 μs. The pulses were run at 1 Hz, and typically 500 pulses were averaged to improve signal to noise. We verified that the time dependence of the free-field decay of the signal was independent of the field from 600 to 4000 V/cm. Sample buffer molarity was fixed at 10 mM in order to minimize any heating artifacts of the electric pulses.

Singlet Depletion Anisotropy Measurements. In singlet depletion anisotropy decay (SDAD), a pulsed laser is used to excite a DNA-bound dye from its singlet ground state to its singlet excited state. This dye singlet excited state then can cross to its triplet state, which exhibits a long lifetime (milliseconds). As the triplet state gets populated, the absorption signal of the singlet transition is decreased. The absorbance polarization of another laser can be used to monitor the singlet absorption band of the dye either parallel or perpendicular to the excitation polarization. These measurements allow two polarization-dependent absorption signals to be recorded, from which the absorption anisotropy as a function of time can be calculated. This decay behavior (called SDAD) can be related to the rotational diffusion of the DNA. The SDAD measurements reported here were performed on an improved version of an instrument used in previous work (Hogan et al., 1983). The major improvements were the development of real-time subtraction of the parallel and perpendicular absorption changes, which removes common-mode intensity fluctuations in the monitoring laser beam, and the use of tuned dye lasers for both the probe and the monitoring beams. These improvements allowed us to set the excitation wavelength to the 670-nm absorption peak of methylene blue (MB) and to set the monitoring beam only 20 nm away at 650 nm. This feature yields consistent initial anisotropy for MB in glycerol of 0.31, the same value as we obtained for the fluorescence anisotropy of MB in glycerol (unpublished observation). The result of these improvements in our apparatus is not only the greatly increased signal to noise capability but also the reduced sample concentration and volume requirements, and more reliable anisotropy decay curves due to the real-time subtraction of intensity fluctuations.

Results and Discussion

Circular Dichroism and Optical Absorption Measurements.

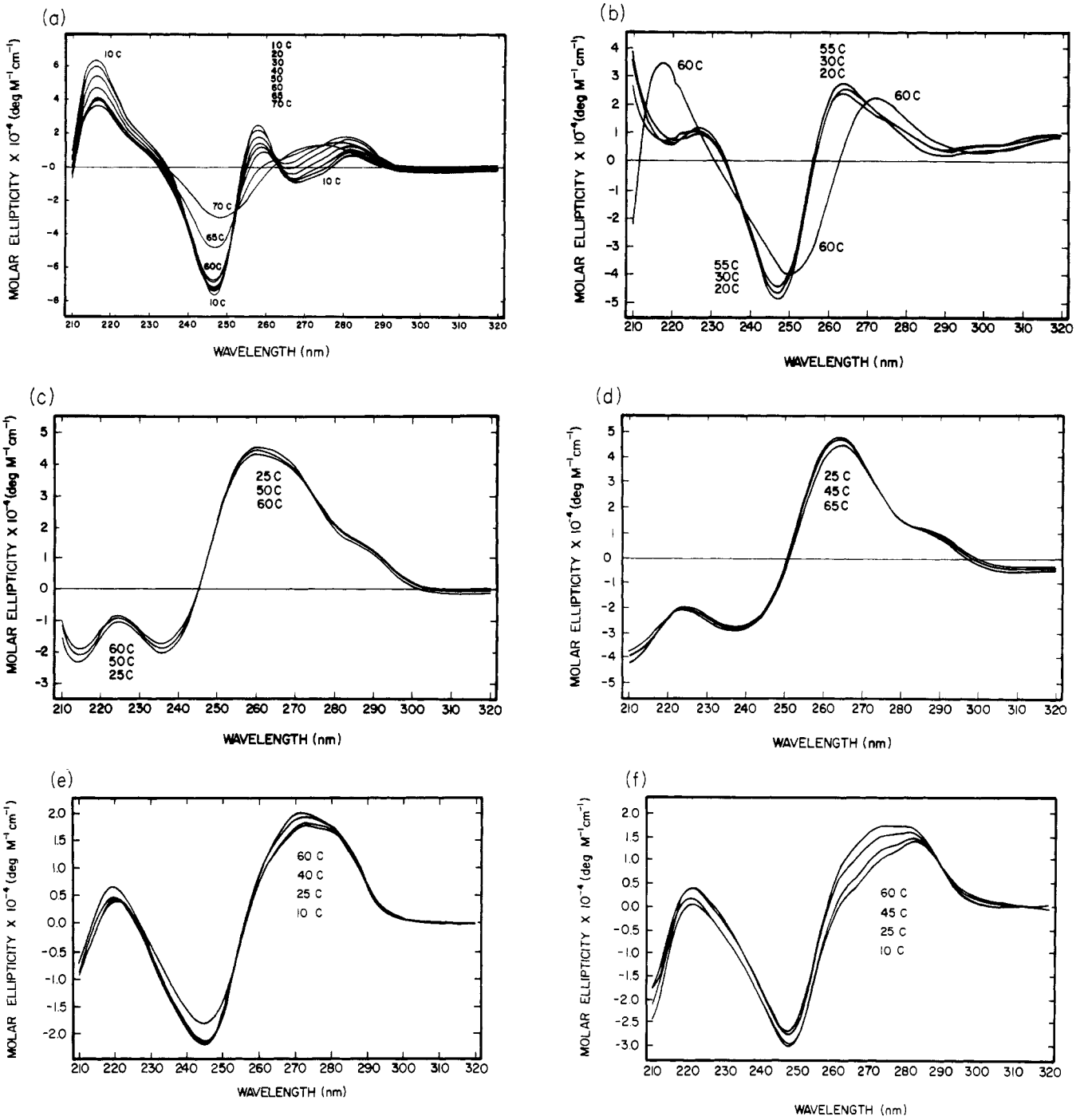

FIGURE 1: CD spectra of DNA fragments as a function of temperature. The buffer for all samples is 90 mM Tris-HCl, pH 7.6, and 0.01 mM EDTA. (a) Poly(dA)·poly(dT) fractionated to a mean length of 780 bp. Three isoelliptic points are maintained from 10 to 65 °C, and the CD values monotonically change with increasing temperature. Poly(dA)·poly(dT) fragments of 520 bp and >1000 bp both exhibit the same spectral changes. Note that, at temperatures below global melting, the CD spectrum is different from the normal B-type CD spectra shown in panels b–f. (b) Poly[d(AT)]·poly[d(AT)] fractionated to a mean length of 810 bp. (c) Poly(dG)·poly(dC) fractionated to a mean length of 400 bp. (d) Poly[d(GC)]·poly[d(GC)] fractionated to a mean length of 460 bp. (e) Calf thymus DNA fragments fractionated to a mean length of 300 bp. (f) kDNA restriction fragment with a chain length of 265 bp.

CD spectra of poly(dA)·poly(dT) as a function of temperature are shown in Figure 1a. We have recorded the CD spectra at 5 °C intervals from 10 to 80 °C. To make the figure more legible, we have plotted only selected temperatures scans in Figure 1a. Three poly(dA)·poly(dT) fragments, 520 bp, 780 bp, and >1000 bp, were studied to evaluate the influence of chain length. Our CD spectra reveal no dependence of this observable on chain length in the range investigated. This observation is consistent with previous CD studies reported by Gennis and Cantor (1972). Inspection of Figure 1a reveals that, below 10 °C, the spectra become almost independent of temperature and are characterized by three maxima at 282, 258, and 216 nm, as well as two minima at 268 and 247 nm. This unusual CD spectrum is similar to that described by Wells and colleagues for long unfractionated dA·dT homopolymer samples at 26 °C (Wells et al., 1970) as well as being similar to the temperature-dependent CD spectra reported by Sarocchi and Guschlbauer (1973) and Greve et al. (1977). Further inspection of the family of curves in Figure 1a reveals that, between 10 and 60 °C, the CD spectrum of poly(dA)·poly(dT) displays a gradual but substantial temperature dependence, characterized by a doubling of the ellipticity in the 265–

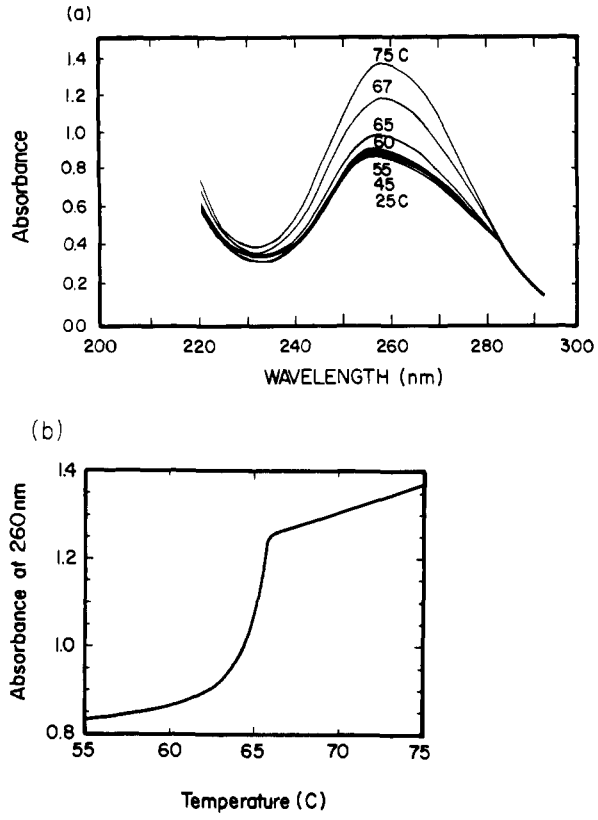

FIGURE 2: (a) UV absorbance spectra for fractionated poly(dA)·poly(dT) fragments (780 bp) at selected temperatures in 90 mM Tris-HCl, pH 7.6, and 0.01 mM EDTA. (b) Temperature-dependent UV absorbance at 260 nm for fractionated poly(dA)·poly(dT) fragments (780 bp) in 90 mM Tris-HCl, pH 7.6, and 0.01 mM EDTA.

285-nm range, a 50% decrease at 216 nm, no change at 247 nm, and three isoelliptic points at 240, 252, and 263 nm. These changes are completely reversible, as assessed by cooling and reheating of the material. Furthermore, this premelting spectral change is not dependent on the poly(dA)·poly(dT) concentration up to 0.5 mM in base pairs. This result is consistent with the premelting process being an intramolecular event.

Recently, Herrera and Chaires (1989) have reported a similar CD premelting transition using unfractionated poly(dA)·poly(dT) (presumably of long length). They suggest that the premelting transition they observe can be induced by daunomycin binding. In addition to their CD measurements, they also report a temperature-dependent optical absorbance change at 286 nm which they propose also results from the premelting event. We do not observe such a thermally induced optical absorbance change at 286 nm, even with our longest dA·dT (>1000 bp) samples (see Figure 2a). However, at *high* base-pair concentrations (1 mM) of poly(dA)·poly(dT), we do observe temperature-dependent UV absorbance changes at 280 and 260 nm (data not shown). One of the UV changes we observe at high base-pair concentrations occurs between 25 and 29 °C, which correlates with the known triple-helix disproportionation equilibrium (Krakauer & Sturtevant, 1968). The other UV change we observe at high base-pair concentrations occurs between 68 and 70 °C and undoubtedly corresponds to global poly(dA)·poly(dT) duplex melting. However, at low base-pair concentrations (50 μM) and low Na^+ concentrations (5 mM), where triple-helix disproportionation is insignificant, we observe, at both 260 and 280 nm, only one transition at 70 °C as well as the same CD changes we find for the 780 and 520 bp samples between 10 and 60 °C. Since Herrera and Chaires did not report the concentrations of their samples, it is not possible to assess if the UV absorbance changes they report may, in part, reflect triple-helix disproportionation. We make this point because Herrera and Chaires based their van't Hoff analysis of the premelting transition in poly(dA)·poly(dT) on their UV absorption data while in this work the corresponding van't Hoff analysis is based on temperature-dependent CD data.

As shown in Figure 1a, above 60 °C, the CD spectrum we measure for poly(dA)·poly(dT) undergoes an abrupt change which most likely corresponds to the onset of the double helix to single strand transition. Similar CD melting behavior for poly(dA)·poly(dT) has been reported by Greve et al. (1977). The assignment of the abrupt temperature-induced event to the global duplex melting is consistent with the UV melting profile we measure for poly(dA)·poly(dT) which exhibits a sharp increase in the 260-nm absorption at about 65 °C (Figure 2b). This value for the melting temperature (T_m) is in good agreement with previous melting studies on poly(dA)·poly(dT) at similar ionic strengths (Marky et al., 1985).

To evaluate if the gradual CD premelting transition we observe is unique to the homopolymer dA·dT sequence element, we also measured CD spectra as a function of temperature for a series of synthetic DNA helices which do not contain the dA·dT homopolymer sequence element and a natural "random sequence" DNA. Inspection of Figure 1b reveals that between 20 and 55 °C the alternating copolymer poly[d(AT)]·poly[d(AT)] does not display a premelting CD change similar to poly(dA)·poly(dT), except for minor alterations in the CD amplitudes. [For poly(dA)·poly(dT), the positions of the CD extrema as well as the CD amplitudes change in the premelting region.] As with the dA·dT homopolymer, the abrupt CD change for poly[d(AT)]·poly[d(AT)] above 60 °C is due to the melting of the duplex, which correlates with the sharp 260-nm absorption increase we observe for poly[d(AT)]·poly[d(AT)] at temperatures above 60 °C. This temperature-dependent CD melting behavior for poly[d(AT)]·poly[d(AT)] is qualitatively consistent with that previously reported by Gennis and Cantor (1972) and Greve et al. (1977). Like poly[d(AT)]·poly[d(AT)], the GC homopolymer (Figure 1c) and the GC alternating copolymer (Figure 1d) also do not display any significant CD changes in the premelting range between 25 and 65 °C.

We also have examined the CD melting behavior of calf thymus (CT) DNA, a naturally occurring DNA duplex. Calf thymus DNA contains no substantial runs of phased dA·dT tracts. Consequently, this duplex might not exhibit the premelting behavior we observe in the homopolymer poly(dA)·poly(dT). Inspection of Figure 1e reveals that this expectation is fulfilled. Prior to global melting, the CD spectra for CT DNA reveal little, if any, temperature dependence. In the aggregate, these results suggest that a homo-A or homo-T tract may be required to induce the structural/conformational form responsible for the CD-detected premelting event we observe. To test this hypothesis directly, we have used CD to study the thermal properties of kDNA fragments which are known to contain phased arrays of A tracts. These results are described below.

We have investigated the temperature dependence of the CD spectrum of kDNA, since it contains phased arrays of A_5·T_5 tracts. Our goal was to assess if kDNA, like poly(dA)·poly(dT), exhibits a premelting temperature dependence prior to global duplex disruption. In this connection, it should be noted that Marini and colleagues (1984) have measured the temperature dependence of the CD spectrum of a phased kDNA fragment and observed some spectral changes. How-

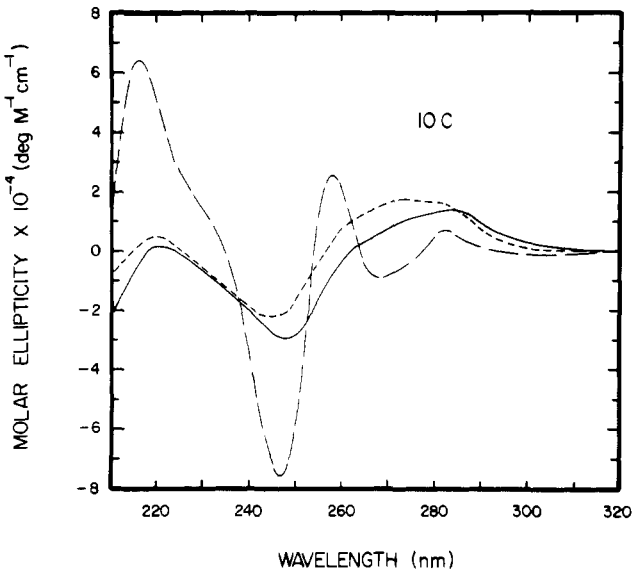

FIGURE 3: CD spectra of poly(dA)·poly(dT) (--), calf thymus DNA (—), and kDNA (---) at 10 °C. Note the large variation in the CD spectra of these different sequences below 260 nm, but the relative scaling that occurs between 270 and 300 nm. See Figure 1 legends for solution conditions.

ever, at the time, they did not examine the temperature dependence of other DNA duplexes so that a meaningful comparison was not possible. In this work, we have measured the CD spectra of a kDNA fragment every 5 °C, between 10 and 60 °C. Figure 1f shows the results of these measurements with only a few selected temperatures presented for the sake of clarity. Inspection of Figure 1f reveals that at low temperature kDNA exhibits an unusual CD spectrum which is different from poly(dA)·poly(dT) or calf thymus DNA (see Figure 3). Significantly, however, in the preglobal melting region, kDNA shows a much stronger temperature dependence than any of the other duplex systems, with the exception of poly(dA)·poly(dT). Above 50 °C, the CD of kDNA becomes similar to that of CT DNA.

The above data suggest that duplexes with homo oligo(dA)·oligo(dT) tracts [e.g., poly(dA)·poly(dT) and kDNA] can exhibit a unique equilibrium below the global melting point of the host duplex. To more clearly illustrate this "premelting" behavior, we have plotted the temperature-dependent CD signals at selected wavelengths for poly(dA)·poly(dT) and kDNA. Figure 4a shows the ellipticity change for poly(dA)·poly(dT) as a function of temperature at 282 and 247 nm, respectively. Note that the ellipticity at 247 nm behaves in a manner similar to the 260-nm UV absorption melting profile. Thus, we propose that the CD signal at 247 nm mainly monitors the global duplex to single strand transition. On the other hand, the CD signal at 282 nm, which changes gradually from 10 to 60 °C, monitors a unimolecular premelting transition between at least two subforms of the helix.

Similar CD melting curves at 248 and 282 nm can be constructed from the temperature-dependent CD data we have measured for our kDNA fragments. Figure 4b shows such a plot. Inspection of this figure reveals a gradual "premelting" CD change at 282 nm and a more abrupt CD change at 248 nm which undoubtedly corresponds to global duplex melting. The striking similarity between these two sets of CD melting data for poly(dA)·poly(dT) and kDNA strongly suggests that the structural/conformational anomalies of poly(dA)·poly(dT) are related to similar changes in kDNA.

Gel Electrophoresis. We have measured the electrophoretic mobility of kDNA as a function of temperature. With increasing temperature, the mobility of kDNA becomes less retarded and approaches that of a linear control. This result agrees with the studies of Marini et al. (1984) on the 414 bp fragment of *Leishmania tarentolae* kinetoplast. Figure 5 shows the gel mobility of our kDNA fragment as a function of temperature, normalized by the mobility of a random fragment of the same length in a 7% polyacrylamide gel. As a control, we have monitored the electrophoresis of DNA restriction fragments from a *Hpa*II digest of pBR322 from 4 to 55 °C. Over this range of temperatures we find that the relative mobility is constant (data not shown). Therefore, we conclude

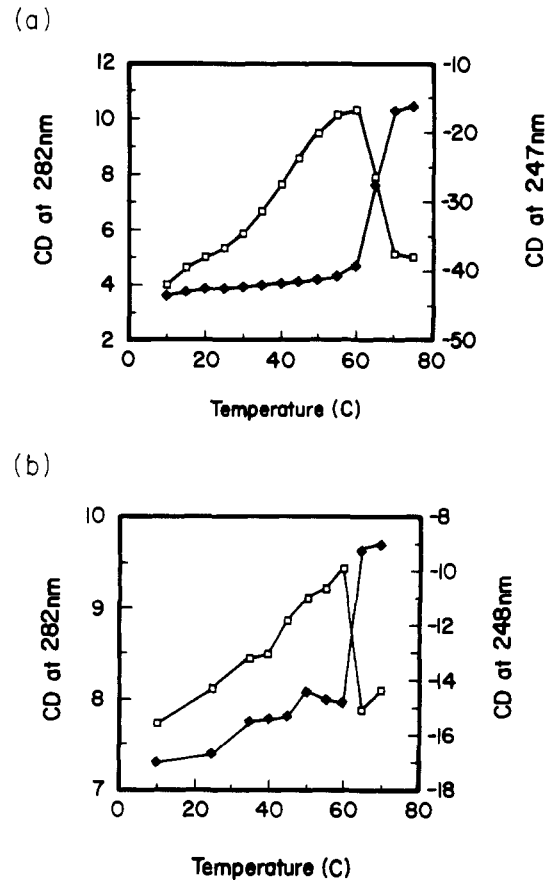

FIGURE 4: CD signals (in millidegrees) at 247 or 248 nm (◆) and 282 nm (□) plotted as a function of temperature. (a) Poly(dA)·poly(dT). (b) kDNA.

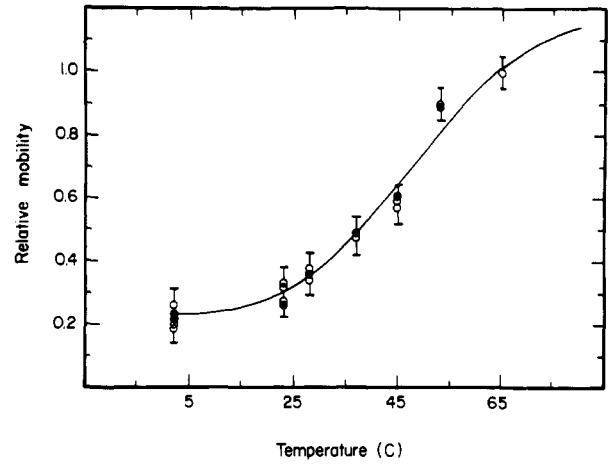

FIGURE 5: Relative gel mobility of the kDNA fragment as a function of temperature in a 7% polyacrylamide gel electrophoresed in 45 mM Tris–borate buffer, pH 8, and 1 mM EDTA. The relative mobility at each temperature T_i was determined by the mobility of kDNA divided by the mobility of a marker DNA fragment of the same length.

that the mechanism of DNA electrophoresis in a 7% polyacrylamide gel matrix is not itself temperature dependent. This suggests that the change in the anomalous gel mobility of kDNA reflects a temperature-induced variation in the DNA conformation. Note the similarity of the temperature dependence of the gel mobility and the temperature dependence of the 282-nm CD signal for poly(dA)·poly(dT) in the preglobal melting range. This similarity suggests that the same feature that causes the unusual electrophoresis properties of kDNA in gels also is responsible for the anomalous CD spectrum of poly(dA)·poly(dT) and its strong temperature dependence prior to global melting. In the sections that follow, we examine the dynamic aspects of this premelting event.

Singlet Depletion Anisotropy Measurements. Singlet depletion anisotropy decay (SDAD) is quite often confused with fluorescence anisotropy decay. Briefly, SDAD uses the creation of long-lived triplet states of intercalated dye molecules to measure motion over a much larger time range than fluorescence anisotropy. Since DNA is a very long, thin, flexible molecule the Brownian dynamics of the molecule cover many decades of time and are highly nonexponential in form. Thus, any technique that claims to observe a substantial fraction of the relevant motions of the molecule must be capable of spanning very large time ranges. Although the SDAD method requires an intercalating dye probe (methylene blue, MB), the dye is present in tracer quantities (less than 1 dye per 100 bp). The data of greatest interest in our measurements span a dynamic range from 0.05 to 2 μs; that is, the region of the collective twisting and bending modes in the helix (Allison & Schurr, 1979). In this time range, DNA motions span many base pairs, and the local structural changes that occur at the dye intercalation site should not significantly perturb the collective motions of interest. The absence of significant dye-induced perturbations has been confirmed from comparisons between different dye probes (Wang et al., 1982) and by the observation that SDAD measurements are independent of the dye probe density in the range from 1/200 to 1/50 dye/(base pairs). It should be noted that SDAD has the potential to measure both the local torsional and the Young's modulii of the helix. Furthermore, it is sensitive to the conformation of the molecule through the diffusion tensor. The actual disentanglement of the data is, of course, very involved and is an unsolved problem at present. In this section we will not attempt to prove one model over another, but instead we will use the technique as a semiqualitative indicator of structural changes in the polymers.

Panels a and b of Figure 6 show typical SDAD data for 450 bp fragments of poly(dG)·poly(dC) versus poly[d(GC)]·poly[d(GC)] and for poly(dA)·poly(dT) versus poly[d(AT)]·poly[d(AT)], respectively. The signal to noise of these measurements is equivalent to the best fluorescence data (Wu et al., 1987) but covers a much greater time range. Control experiments (not shown) confirm that the maximum anisotropy observed is independent of the laser excitation energy and the monitoring wavelength. Note that at long times the two AT polymer pairs decay significantly faster than the two GC polymer pairs. Consistent with our previous work (Hogan & Austin, 1987), these data suggest that the AT sequences have considerably greater bending flexibility than the GC fragments. This stiffness difference is particularly clear for the slowest motions of the helix (greater than 1 μs), which are dominated by the longest mode bending motions. This variation of rigidity with sequence might be expected in light of the different melting points of the homopolymers as well as their different CD spectra (compare panels a–d of Figure 1).

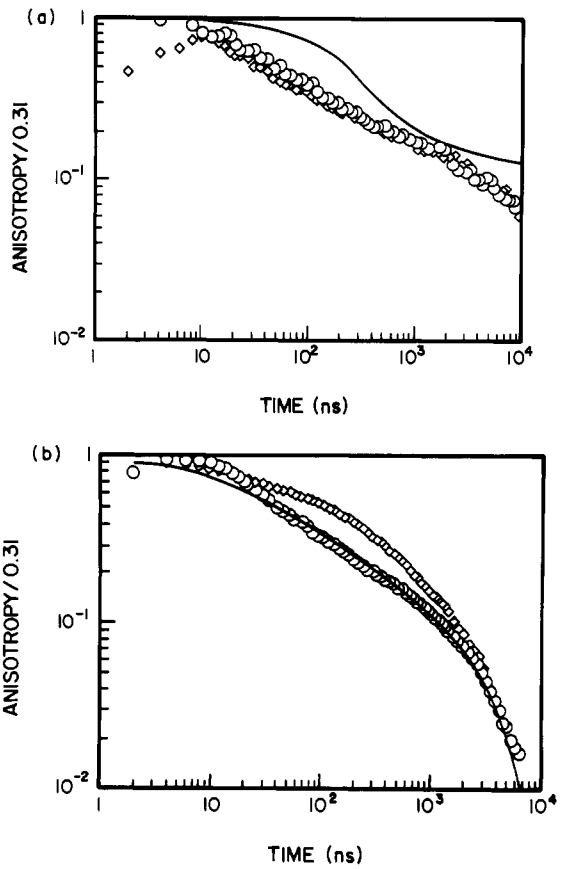

FIGURE 6: SDAD of fractionated DNA fragments (450 bp) at 5 °C as a function of time in 10 mM Tris-HCl, pH 7.5, and 0.01 mM EDTA. The maximum anisotropy of MB is 0.31; hence the anisotropy values have been normalized by using this value. (a) Poly(dG)·poly(dC) (◇) and poly[d(GC)]·poly[d(GC)] (○). The solid line is the expected anisotropy decay of a rigid rod of the same length (450 bp = 1350 Å) and diameter (26 Å) as these samples. (b) Poly(dA)·poly(dT) (◇) and poly[d(AT)]·poly[d(AT)] (○). The solid line is a dynamics simulation using the Schurr model (Allison & Schurr, 1979) and the consensus values of the A·T rigidity as determined by Hogan and Austin (1987).

At low temperature, the dynamics of poly(dA)·poly(dT) are different from the dynamics of poly[d(AT)]·poly[d(AT)], and poly(dA)·poly(dT) shows a strong premelting CD temperature dependence that is absent in poly[d(AT)]·poly[d(AT)]. Consequently, it is of interest to ask if poly(dA)·poly(dT) also shows aberrant temperature dependence in its Brownian dynamics. In fact, we find the temperature dependence of the poly(dA)·poly(dT) anisotropy decay to be unusual. To conduct these experiments, we used short DNA fragments (145 bp) due to the loss of triplet yield at elevated temperatures. Figure 7a shows the temperature dependence of poly(dA)·poly(dT) anisotropy decay from 10 to 50 °C while Figure 7b shows the temperature dependence of the SDAD for poly[d(AT)]·poly[d(AT)] over the same range. The data in these figures show that the anisotropy decay of poly(dA)·poly(dT) exhibits a highly unusual temperature dependence which does not converge to the expected decay of poly[d(AT)]·poly[d(AT)] at temperatures over 40 °C, as one might expect from the CD measurements.

Since the kDNA fragment contains phased regions of homo oligo(dA)·oligo(dT), one might expect to find large differences in the dynamics between kDNA and "random" sequence DNA [if the short oligo(dA)·olgio(dT) tracts in kDNA form the same unusual structure as they do in the poly(dA)·poly(dT) homopolymer]. In Figure 8 we plot the SDAD of three DNA fragments of basically the same length: kDNA (219 bp), sea

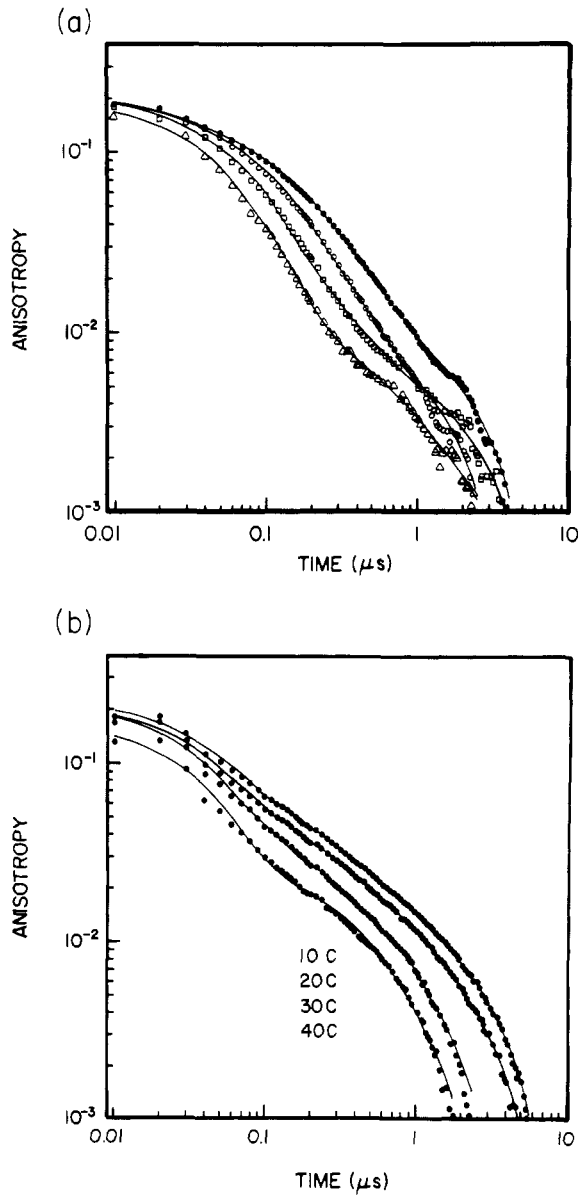

FIGURE 7: Anisotropy decay of A·T fragments (145 bp) as a function of temperature in 10 mM Tris-HCl, pH 7.5, and 0.01 mM EDTA. (a) Poly(dA)·poly(dT) at (●) 10 °C, (○) 20 °C, (□) 30 °C, and (△) 40 °C. Note that the anisotropy decay functional shape changes with temperature and that the longest time constant of the decay is surprisingly independent of temperature, although the faster parts of the decay show the increase in anisotropy decay with increasing temperature. (b) Poly[d(AT)]·poly[d(AT)] at 10 °C (top curve) to 40 °C (bottom curve). Note that the shape of the anisotropy decay curve is relatively unchanged and that the effect of increased temperature seems to be basically a general decrease in the anisotropy decay time.

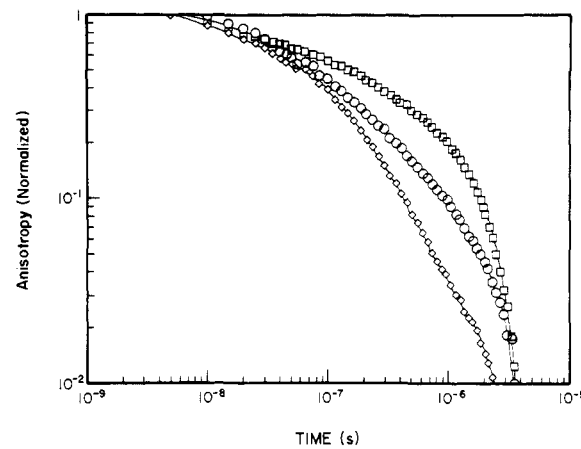

FIGURE 8: SDAD measurements in 10 mM Tris-HCl, pH 7.5, and 0.01 mM EDTA at 5 °C for poly[d(AT)]·poly[d(AT)] with a mean length of 210 bp (◇), an *Aval*–*Aval* restriction fragment of sea urchin 5S DNA with 209 bp (○), and a *Bam*HI–*Bam*HI insert of kDNA with 219 bp (□).

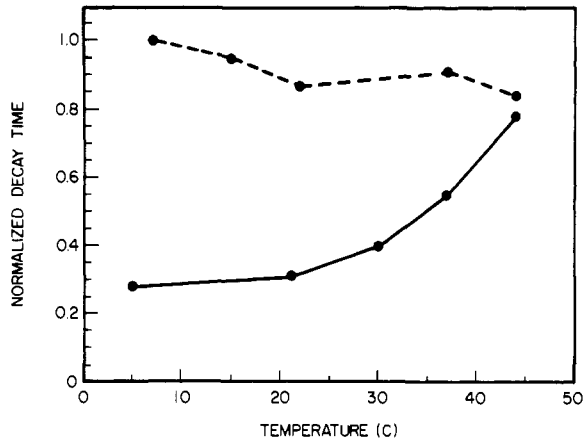

FIGURE 9: Analysis of the temperature dependence of the observed longest time of birefringence decay for the sea urchin fragment (---) and the kDNA fragment (—). A two-exponential fitting program is used to fit the data. Each point is the longest time of the two decay components, which always is at least 90% of the total amplitude of the total signal. The decay times are corrected for viscosity η/T effects due to increasing temperature and normalized to sea urchin's time at 5 °C.

urchin DNA (209 bp) of essentially random sequence, and poly[d(AT)]·poly[d(AT)] (highly fractionated mean, 210 bp). Inspection of Figure 8 reveals that the kDNA fragment exhibits a highly unusual anisotropy decay which is markedly different from either poly[d(AT)]·poly[d(AT)] or "normal" random sequence DNA.

Birefringence Measurements. Electric birefringence measurements have the potential to measure the long-time tumbling motions of DNA fragments (Ding et al., 1972) and in particular are sensitive both to the rigidity of the helix (Hagerman & Zimm, 1981; Hagermann, 1981) and to any static curvature of the helix (Mellado & De La Torre, 1982; Hagerman, 1984). The data set collected in this part of the experiment is not as extensive as the set collected in the previous two sections. We wanted to compare the temperature dependence of the birefringence decay of poly(dG)·poly(dC), poly[d(GC)]·poly[d(GC)], poly(dA)·poly(dT), poly[d(AT)]·poly[d(AT)], and kDNA fragments. However, for nonrestriction fragment DNA preparations the width of the length distribution is particularly disturbing for birefringence measurements, since long fragments with their corresponding large dipole moments align to a greater degree than short fragments. Hence, in the absence of either very narrow or no distributions of the DNA fragment length it is difficult to get accurate measurements for the long-term rotation times that are not strongly heterogeneous. The one sample where it is possible to get monodisperse data is in the case of the kDNA fragment, which was a restriction fragment and monodisperse, and could be accurately compared to a monodisperse restriction fragment of random sequence of the same length. We have carried out electric birefringence measurements in order to determine if the anomalous properties of kDNA would exhibit the same strong temperature dependence that the gels, CD, and SDAD measurements show. Figure 9 shows the longest time component of the birefringence decay for the kDNA fragment (219 bp) and a sea urchin restriction fragment (209 bp) as a function of temperature. It is clear that the kDNA fragment shows a strong temperature dependence, with an

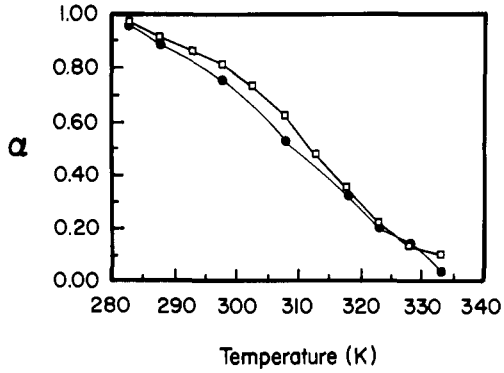

FIGURE 10: van't Hoff plot of α versus temperature for poly(dA)·poly(dT) (□) and kDNA (●). These points were evaluated from the CD signals at 282 nm (see Figure 4).

increasing corrected birefringence decay time vs temperature. By contrast, the random sequence fragment varies from flat to slightly decreasing, as one would expect for a small decrease in the Young's modulus with temperature.

Data Analysis

Circular Dichroism. Because of the well-defined isoelliptic points for the premelting transition in poly(dA)·poly(dT), the CD data of Figure 1a may be described by a temperature-dependent equilibrium between two distinct forms of the double-stranded DNA helix, each with its own CD spectral properties (Ts'o, 1974). If we define α to be the ratio of the concentrations of the low- and high-temperature species, then the 282-nm CD versus T data in Figure 4a can be converted graphically into an α versus T melting curve as shown in Figure 10 (Cantor & Schimmel, 1980). The van't Hoff enthalpy of this "premelting" transition then can be calculated from the general form of the van't Hoff equation (Cantor & Schimmel, 1980; Marky & Breslauer, 1987):

$$\Delta H_{vH} = (2 + 2n)RT_{pm}^2(d\alpha/dT)_{T_{pm}}$$

where n is the molecularity of the transition and T_{pm} is the premelting temperature at $\alpha = 0.5$. Since the premelting transition is intramolecular, $n = 1$. From the α versus T plot (Figure 10) we obtain an apparent T_{pm} of 312 K or 39 °C for the premelting transition, and from the slope at T_{pm} we obtain an apparent van't Hoff enthalpy (ΔH_{vH}) of 20.5 ± 5.0 kcal/mol per cooperative unit. (The error in this treatment primarily reflects the difficulty in defining the transition end points in Figure 4a.) This ΔH_{vH} value for the poly(dA)·poly(dT) premelting equilibrium compares favorably with that previously reported by Herrera and Chaires (1989). However, they based their van't Hoff analysis on temperature-dependent UV absorption data at 286 nm while our van't Hoff analysis is based on temperature-dependent CD data at 282 nm. Significantly, as also shown in Figure 10, we can derive a similar α versus T premelting curve for kDNA. This similarity in the premelting behaviors of poly(dA)·poly(dT) and kDNA suggests that at low temperatures (<37 °C) these two duplexes assume similar altered, non-B-form structures.

In the case of kDNA, it is interesting to ask if the CD spectrum of kDNA is a simple linear superposition of poly(dA)·poly(dT) plus "normal" random sequence DNA. It has been observed that the CD spectra of DNA of variable sequence can be reproduced with good accuracy by summing the CD spectra corresponding to nearest-neighbor pairings (Gray & Tinoco, 1970; Wells et al., 1970; Arnott, 1975). If, indeed, the oligo(dA)·oligo(dT) sequences within kDNA form a structure similar to poly(dA)·poly(dT), then it should be possible to calculate the CD spectrum of kDNA. However, Figure 3 shows that the CD spectra of the dA·dT, calf thymus, and kDNA species are so different in the short-wavelength range that it is unlikely that any sort of a linear summation would yield the kDNA CD spectrum. Thus, while the A·T sequence within kDNA has an aberrant structure, it may not be identical with the aberrant structure of poly(dA)·poly(dT).

Singlet Depletion Anisotropy and Birefringence Decay. The detailed analysis of the anisotropy decay of the fragments will be given in a separate paper. In this paper we use three exponentials to fit the SDAD data and two exponentials to fit the EBD data. The longest relaxation time of each SDAD curve is due to pure bending motions. We use this longest relaxation time as a rough characterization of the anisotropy decay and compare it with the longest time of the birefringence decay. The program we used for these exponential fits employs a modified least-squares/steepest descent algorithm. Standard deviations per point were determined by pretrigger noise. The reduced χ^2 values of the final fits were less than 2. Since the general law for any sort of an overdamped Brownian motion in solution is that it should scale as η/T, we have multiplied the time constants by T/η in order to compensate for this effect. The time constants then were normalized by dividing by the (corrected) time constant at 5 °C.

Figure 11a shows a plot of these normalized time constants which now are dimensionless. Inspection of Figure 11a reveals that the rigidity of the poly[d(AT)]·poly[d(AT)] versus temperature is not changed so that the apparent increase in anisotropy decay rate is purely hydrodynamic and statistical in nature. Note also that the poly[d(AT)]·poly[d(AT)] fragment is indeed significantly more flexible than a rigid rod. This is clear from the rigid rod plot in the figure. To establish the rigid rod plot, we took the longest decay time expected from a rigid rod from the Broersma empirical relations (Broersma, 1960), divided by the corrected 5 °C data, and successively corrected for T/η effects. Note that this line remains roughly a factor of 2 greater than the data for the poly[d(AT)]·poly[d(AT)] fragment over the entire temperature range. The situation is quite different for poly(dA)·poly(dT) (Figure 11b). The longest anisotropy decay time *increases* with increasing temperature when the corrections are made, indicating that some sort of a structural or elastic change in the helix is occurring. It is gratifying to note that the changes occur over the same temperature range in which premelting effects are seen in the CD spectra.

We observe similar temperature effects in the birefringence data. As in the SDAD decay data, the time constants of the observed motions must be scaled by the T/η. In Figure 9 we plot the corrected times of the birefringence decay, normalized to the 5 °C value. The random sequence fragment shows a very weak decrease in the longest relaxation time, indicating a very small decrease in the Young's modulus with temperature, in agreement with other measurements of the temperature of the persistance length (Gray & Tinoco, 1970; Hagerman, 1981). However, the kDNA shows very unusual properties: the longest time constant actually *increases* with increasing temperature and, at the highest temperature studied, has almost the same rotational time as the random sequence fragment. Again, these effects are in close correlation with the CD anomalies.

Evidence from Dye Binding. In terms of ligand recognition of and influence on the oligo(dA) sequence element, Wilson and colleagues have shown that the intercalating drug, propidium iodide, binds cooperatively to poly(dA)·poly(dT). By contrast, under the same conditions, propidium iodide binding

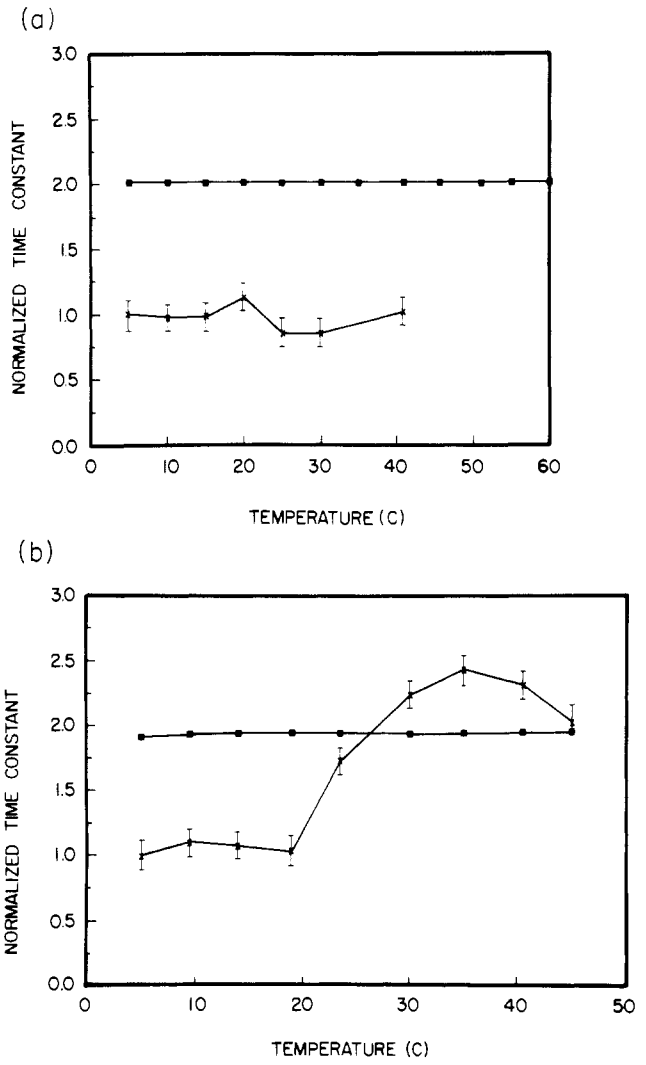

FIGURE 11: Temperature dependence of the normalized longest time of the SDAD process for 145 bp fragments. A three-exponential fitting program is used to fit the data. Each point is the longest time of the three components, which corresponds roughly to the end-to-end tumbling time of the entire fragment. Each normalized time is corrected for viscosity effects and normalized to the 5 °C value. The normalized longest time for a rigid rod also is shown. (a) Poly[d-(AT)]·poly[d(AT)] (×); rigid rod (■). (b) Poly(dA)·poly(dT) (×); rigid rod (■).

to poly[d(AT)]·poly[d(AT)] and other sequences is non-cooperative (Wilson et al., 1985). The authors suggest that their data can be interpreted by assuming a model in which ligand intercalation into poly(dA)·poly(dT) is allosterically coupled to a binding-induced conformational equilibrium. The Breslauer group has reported drug–DNA binding thermodynamics which are consistent with this interpretation (Marky et al., 1985; Breslauer et al., 1987; Chou et al., 1987). Specifically, the DNA binding enthalpies of ethidium bromide, daunomycin, distamycin, and netropsin were measured using calorimetric techniques. The first two ligands are widely studied as models for intercalative drug binding, while the latter two ligands bind in the minor groove and have been studied as models for sequence-specific peptides. For each of the four drugs, the Breslauer group found that binding to poly(dA)·poly(dT) is characterized by enthalpies and entropies which are qualitatively different from those measured for binding to poly[d(AT)]·poly[d(AT)]. To be specific, at 25 °C the binding of each drug to poly(dA)·poly(dT) is entropy driven while the binding of the corresponding drug to poly-[d(AT)]·poly[d(AT)] is enthalpy driven. It was suggested by Breslauer and co-workers (Marky et al., 1985; Breslauer et al., 1987; Chou et al., 1987) that the large positive entropy change upon binding to poly(dA)·poly(dT) may reflect both/either a drug-induced conformational change in the DNA substructure of poly(dA)·poly(dT) and/or a change in DNA hydration. In the context of this work, it may be argued that the anomalous thermodynamic data that the Breslauer group has measured for drug binding to poly(dA)·poly(dT) reflects a drug-induced alteration in the secondary structure initially assumed by poly(dA)·poly(dT). Quite recently, Herrera and Chaires (1989) reported thermodynamic behavior consistent with that found by the Breslauer group (Breslauer et al., 1987) for daunomycin binding to the poly(dA)·poly(dT) and poly-[d(AT)]·poly[d(AT)] duplexes. They propose an explanation that is consistent with that originally suggested by Wilson et al. (1985) and present data that quantitatively supports the model of a daunomycin-induced conformational change in poly(dA)·poly(dT). We agree with the conclusions of the Wilson, Breslauer, and Chaires groups and suggest that the equilibrium which each of these groups have inferred from their ligand binding thermodynamics is identical with the premelting equilibrium that we have detected by CD analysis in the ligand-free structures of poly(dA)·poly(dT) and kDNA.

Conclusions

On the basis of the static and dynamic data presented here and the corroborating data from other laboratories, we suggest that, under physiological conditions of salt and temperature and in the absence of external mechanical stress, the oligo-(dA)·oligo(dT) sequence element is capable of a conformational equilibrium between at least two helical forms prior to global duplex melting. These two "premelting" states are distinguished by their CD spectra, Brownian dynamics, and their capacity to function as a drug or enzyme binding site. Consistent with previously proposed models (Wilson et al., 1985; Breslauer et al., 1987; Herrera & Chaires, 1989) we suggest that this premelting equilibrium may serve as the basis for ligand binding allostery which has been inferred at oligo(dA)·oligo(dT) sites in vitro and may, in part, reflect the thermal disruption of "bent" DNA.

Acknowledgments

We thank Dr. Paul Englund for generously providing us with the kinetoplasmid pPK201/CAT and Dr. Robert Simpson for the sea urchin plasmid p5S207.

References

Alexeev, D. G., Lipanov, A. A., & Skuratovskii, I. (1987) *Nature 325*, 821–823.
Allison, S. A., & Schurr, J. M. (1979) *Chem. Phys. 41*, 35–59.
Arnott, S. (1975) *Nucleic Acids Res. 2*, 1493–1502.
Brahams, S., Brahms, J., & van Holde, K. E. (1976) *Proc. Natl. Acad. Sci. U.S.A. 73*, 3453–3457.
Breslauer, K. J., Remeta, D. P., Chou, W. Y., Ferrante, R., Curry, J., Zaunczkowski, D., Snyder, J. G., & Marky, L. A. (1987) *Proc. Natl. Acad. Sci. U.S.A. 84*, 8922–8926.
Broersma, S. (1960) *J. Chem. Phys. 32*, 1626–1631.
Cantor, C. R., & Schimmel, P. R. (1980) *Biophysical Chemistry*, Part II, p 384, Freeman, CA.
Chou, W. Y., Marky, L. A., Zaunczkowski, D., & Breslauer, K. J. (1987) *J. Biomol. Struct. Dyn. 5*, 345–359.
Coll, M., Frederick, C. A., Wang, A. H. J., & Rich, A. (1987) *Proc. Natl. Acad. Sci. U.S.A. 84*, 8385–8389.
Crothers, D. M., Hibers, C. W., & Shulman, R. G. (1973) *Proc. Natl. Acad. Sci. U.S.A. 70*, 2899–2901.

Diekmann, S., & Wang, J. C. (1985) *J. Mol. Biol. 186*, 1–11.
Ding, R.-W., Rill, R., & van Holde, K. E. (1972) *Biopolymers 11*, 2109–2124.
Doty, P., Boedtker, H., Fresco, J. R., Haselkorn, R., & Litt, M. (1959) *Proc. Natl. Acad. Sci. U.S.A. 45*, 482–499.
Erfurth, S. C., & Peticolas, W. L. (1975) *Biopolymers 14*, 247–265.
Frederick, C. A., Grable, J., Melia, M., Samucki, C., Jen-Jacobson, L., Wang, B. C., Greene, P., Boyer, H., & Rosenberg, J. M. (1984) *Nature 309*, 327–331.
Fresco, J. R. (1961) *Tetrahedron 13*, 185–197.
Freund, A. M., & Bernardi, G. (1963) *Nature (London) 200*, 1318–1320.
Gennis, R. B., & Cantor, C. R. (1972) *J. Mol. Biol. 65*, 381–399.
Gray, D. M., & Tinoco, I. (1970) *Biopolymers 9*, 223–244.
Greve, J., Maestre, M. F., & Levin, A. (1977) *Biopolymers 16*, 1489–1504.
Hagerman, P. J. (1981) *Biopolymers 20*, 1503–1535.
Hagerman, P. J. (1984) *Proc. Natl. Acad. Sci. U.S.A. 81*, 4632–4636.
Hagerman, P. J., & Zimm, B. H. (1981) *Biopolymers 20*, 1481–1502.
Herrera, J. E., & Chaires, J. B. (1989) *Biochemistry 28*, 1993–2000.
Hogan, M. E., & Austin, R. H. (1987) *Nature 329*, 263–266.
Hogan, M. E., LeGrange, J., & Austin, R. H. (1983) *Nature 304*, 752–754.
Hogan, M. E., Rooney, T. F., & Austin, R. H. (1987) *Nature 328*, 554–557.
Kitchin, P. A., Klein, V. A., Gann, K. L., Rauch, C. A., Kang, D. S., Wells, R. D., & Englund, P. T. (1986) *J. Biol. Chem. 261*, 11302–11309.
Krakauer, H., & Sturtevant, J. M. (1968) *Biopolymers 6*, 491–519.
Lazurkin, Y. S., Frank-Kamenetskii, M. K., & Trifonov, E. F. (1970) *Biopolymers 9*, 1253–1306.
Liu-Johnson, H. N., Gartengerg, M. R., & Crothers, D. M. (1986) *Cell 47*, 995–1005.
Marini, J. C., Effron, P. N., Goodman, T. C., Singleton, C. K., Wells, R. D., Wartell, R. M., & Englund, P. T. J. (1984) *Biol. Chem. 259*, 8974–8979.
Marky, L. A., & Breslauer, K. J. (1987) *Biopolymers 26*, 1601–1620.
Marky, L. A., Curry, J., & Breslauer, K. J. (1985) in *Molecular Basis of Cancer* (Rein, R., Ed.) pp 155–173, Alan Liss, New York.
Maroun, R. C., & Olson, W. K. (1988) *Biopolymers 27*, 585–603.
Mellado, P., & De La Torre, J. G. (1982) *Biopolymers 21*, 1857–1871.
Nelson, H. C. M., Finch, J. T., Luisi, B. F., & Klug, A. (1987) *Nature 330*, 221–226.
Olson, W. K., Sarma, M. H., Sarma, R. H., & Sundaralingam, M., Eds. (1987) *Structure and Expression, Volume 3: DNA Bending and Curvature*, Adenine Press, Schenectady, NY.
Palecek, E. (1976) *Prog. Nucleic Acad Res. Mol. Biol. 18*, 151–213.
Sarocchi, M. T., & Guschlbauer, W. (1973) *Eur. J. Biochem. 34*, 232–240.
Simpson, R. T., & Stafford, D. N. (1983) *Proc. Natl. Acad. Sci. U.S.A. 80*, 50–55.
Srinivasan, A. R., Torres, R., Clark, W., & Olson, W. K. (1987) *J. Biomol. Struct. Dyn. 5*, 459–496.
Ts'o, P. O. P. (1974) *Basic Principles in Nucleic Acid Chemistry*, Vol. II, Academic Press, New York.
Ts'o, P. O. P., & Helmkamp, G. (1961) *Tetrahedron 13*, 198–207.
van Hippel, P. H., & Wong, K. Y. (1971) *J. Mol. Biol. 61*, 587–613.
Wang, J., Hogan, M. E., & Austin, R. H. (1982) *Proc. Natl. Acad. Sci. U.S.A. 79*, 5896–5900.
Wells, R. D., Larson, J. E., Grant, R. C., Shortle, B. E., & Cantor, C. R. (1970) *J. Mol. Biol. 54*, 465–497.
Wilson, W. D., Wang, Y. H., Krishnamoorthy, C. R., & Smith, J. C. (1985) *Biochemistry 24*, 3991–3999.
Woo, H. M., & Crothers, D. M. (1984) *Nature 308*, 509–513.
Wu, P., Fujimoto, B. S., & Schurr, J. M. (1987) *Biopolymers 26*, 1463–1488.